Cyanobacterial growth and morphology are influenced by carboxysome positioning and temperature

Rees Rillema[a*], Joshua S. MacCready[a], Anthony G. Vecchiarelli[a#]

[a] Department of Molecular, Cellular, and Developmental Biology, University of Michigan, Ann Arbor, MI, USA.

* Present Address: BioMolecular Science Program, Michigan State University, East Lansing, MI, USA.

Running Title: Carboxysome mispositioning alters cell physiology

[#]**Address correspondence to Anthony G. Vecchiarelli:** ave@umich.edu

ABSTRACT: Cyanobacteria are the prokaryotic group of phytoplankton responsible for a significant fraction of global CO_2 fixation. Like plants, cyanobacteria use the enzyme Ribulose 1,5-bisphosphate Carboxylase/Oxidase (RuBisCO) to fix CO_2 into organic carbon molecules via the Calvin-Benson-Bassham cycle. Unlike plants, cyanobacteria evolved a carbon concentrating organelle called the carboxysome - a proteinaceous compartment that encapsulates and concentrates RuBisCO along with its CO_2 substrate. In the rod-shaped cyanobacterium *Synechococcus elongatus* PCC7942, we recently identified the McdAB system responsible for uniformly distributing carboxysomes along the cell length. It remains unknown what role carboxysome positioning plays with respect to cellular physiology. Here, we show for the first time that a failure to distribute carboxysomes leads to a temperature-dependent decrease in cell growth rate, cell division arrest, cell elongation, asymmetric cell division, and a significant reduction in cellular levels of RuBisCO. Unexpectedly, we also report that even wild-type *S. elongatus* undergoes filamentous growth at the cool, but environmentally-relevant, growth temperature of 20°C. The findings suggest that carboxysome positioning by the McdAB system functions to maintain the carbon-fixation efficiency of RuBisCO by preventing carboxysome aggregation, which is particularly important at temperatures where rod-shaped cyanobacteria adopt a filamentous morphology.

IMPORTANCE: Photosynthetic cyanobacteria are responsible for almost half of global CO_2 fixation. Due to eutrophication, rising temperatures, and increasing atmospheric CO_2 concentrations, cyanobacteria have recently gained notoriety for their ability to form massive blooms in both freshwater and marine ecosystems across the globe. Like plants, cyanobacteria use the most abundant enzyme on Earth, RuBisCO, to provide the sole source of organic carbon

required for its photosynthetic growth. Unlike plants, cyanobacteria have evolved a carbon-concentrating organelle called the carboxysome that encapsulates and concentrates RuBisCO with its CO_2 substrate to significantly increase carbon-fixation efficiency and cell growth. We recently identified the positioning system that distributes carboxysomes in cyanobacteria. However, the physiological consequence of carboxysome mispositioning in the absence of this distribution system remains unknown. Here we find that carboxysome mispositioning triggers temperature-dependent changes in cell growth and morphology as well as a significant reduction in cellular levels of RuBisCO.

INTRODUCTION

Cyanobacteria represent a phylum of diverse prokaryotic organisms where many fundamental biological processes have remained largely understudied. As the evolutionary ancestor of algae and plant chloroplasts, all cyanobacteria perform oxygenic photosynthesis and fix carbon dioxide through the Calvin-Benson-Bassham cycle. Unlike chloroplasts, cyanobacteria encapsulate their RuBisCO and carbonic anhydrase within large (~150 nm) selectively permeable protein-based organelles called carboxysomes. This mechanism generates an environment around RuBisCO that is significantly enriched in CO_2, which increases the carboxylation activity of RuBisCO, while simultaneously reducing photorespiration (1).

In the model rod-shaped cyanobacterium *Synechococcus elongatus* PCC 7942 (hereafter *S. elongatus*), carboxysomes were found to be uniformly distributed down the length of individual cells (2). This equidistant positioning supports equal inheritance of carboxysomes following cell division and maximum diffusion of substrates and products across the carboxysome shell. Carboxysomes are essential for the growth and survival of all cyanobacteria

47 and are responsible for ~35% of global carbon-fixation through atmospheric CO_2 assimilation
48 (Dworkin, 2006; Kerfeld and Melnicki, 2016). However, it remains unknown how the
49 subcellular organization of carboxysomes influences cyanobacterial physiology; a question of
50 considerable ecological, evolutionary, and biotechnological importance.

51 Savage *et. al.* were first to report that a ParA-type ATPase (hereafter McdA
52 - Maintenance of carboxysome distribution A) is required for positioning carboxysomes in *S.*
53 *elongatus* (2). ParA family members have well established roles in the segregation of bacterial
54 chromosomes and plasmids (4, 5). Less studied are ParA family members shown to be required
55 in the positioning of diverse protein complexes, such as those involved in secretion (6, 7),
56 chemotaxis (8–10), conjugation (11), cell division (12, 13), and cell motility (14, 15), as well as
57 bacterial microcompartments (BMCs), such as the carboxysome (2, 16). We recently identified a
58 small novel protein, McdB, responsible for generating dynamic McdA gradients on the nucleoid
59 (16). McdB colocalizes and directly interacts with carboxysomes and removes McdA from the
60 nucleoid in their vicinity. We found that carboxysomes use a Brownian-ratchet mechanism
61 whereby McdB-bound carboxysome motion occurs in a directed and persistent manner toward
62 increased concentrations of McdA on the nucleoid. We also recently found that the McdAB
63 system is widespread among β-cyanobacteria (17); an incredibly diverse and widely distributed
64 phylum of bacteria that display complex morphologies (18). Together, the data suggest that the
65 equidistant positioning of carbon-fixing carboxysomes in cyanobacteria is important, but the
66 physiological consequences of carboxysome mispositioning in the absence of the McdAB system
67 remain unclear.

68 When Savage *et. al.* first identified the McdA requirement for carboxysome positioning,
69 only a minor decrease in CO_2 fixation was found in a Δ*mcdA* strain, but growth at 30°C under

70 ambient CO_2 was the only condition studied (2). Rising sea surface temperatures and coastal
71 eutrophication in marine ecosystems are pervasive effects of climate change (19). Rising
72 temperatures increase enzyme kinetics (20), leading to higher rates of protein synthesis,
73 RuBisCO activity, and photosynthesis (21). Temperature therefore directly influences
74 cyanobacterial growth and metabolic rates (22, 23).

75 Here, we show for the first time that a failure to distribute carboxysomes leads to
76 temperature-dependent decreases in growth rate, cell division arrest, cell elongation, asymmetric
77 cell division, and a significant reduction in cellular levels of RuBisCO. We also report that,
78 unexpectedly, wild-type *S. elongatus* undergoes filamentous growth at 20ºC; an environmentally
79 relevant growth temperature for *S. elongatus* not commonly used in the lab. We propose that
80 carboxysome positioning by the McdAB system functions as part of an autotrophic growth
81 strategy that maintains the carbon-fixation efficiency of RuBisCO by preventing carboxysome
82 aggregation. In the absence of carboxysome positioning or when cells are grown at cooler
83 temperatures, we propose that cell elongation and asymmetric cell division are responses to
84 organic carbon limitation, due to the decreased enzymatic activity of RuBisCO under these
85 conditions.

86

87 **RESULTS**

88 We performed *in vivo* microscopy to determine how carboxysome organization was altered
89 in *mcdA*, *mcdB*, and *mcdAB* deletion strains compared to wild-type *S. elongatus*. In *S. elongatus*,
90 each RuBisCO enzyme is composed of eight Large (RbcL) and eight Small (RbcS) subunits to
91 form $RbcL_8S_8$ (24). Therefore, to image carboxysomes, the fluorescent protein mTQ (monomeric
92 Turquoise2) was fused to the C-terminus of RbcS to make RbcS-mTQ (see Methods for strain

93 construction details). *RbcS-mTQ* was expressed using a second copy of its native promoter
94 (inserted at neutral site 1) in addition to wild-type *rbcS* at its native locus in wild-type cells as
95 well as in the three deletion strains – Δ*mcdA*, Δ*mcdB*, and Δ*mcdAB*. The presence of RbcS-mTQ
96 did not alter growth rate **(Supplemental Figure S1)**. Carboxysomes of *S. elongatus* encapsulate
97 between 800 to 1,500 RuBisCO enzymes (25). Therefore, RbcS-mTQ provided a bright and
98 high-contrast marker for quantifying the subcellular organization of carboxysomes, as previously
99 shown (16). We also performed Phase Contrast imaging to monitor for potential changes in cell
100 morphology, and Chlorophyll fluorescence imaging to verify that cells treated in our analyses
101 were photosynthetically active and therefore viable.
102 In the lab, *S. elongatus* is typically grown at 32ºC; with a doubling time on the order of
103 several hours depending on growth conditions (temperature, light, and CO_2 availability). This
104 was the temperature used in our previous study that identified the McdAB carboxysome
105 positioning system (16). However, *S. elongatus* was recently shown to grow faster at 40ºC (26,
106 27). Therefore, in anticipation of a growth defect in the absence of carboxysome positioning in
107 our Mcd system mutants, we began our studies by growing cultures at 40ºC in constant light
108 under ambient (0.04%) or high (2%) CO_2 concentrations.
109
110 **Carboxysome mispositioning correlates with minor defects in cellular physiology at 40ºC**
111 We first verified that carboxysomes are organized by the McdAB system at 40ºC, as we
112 found previously at 32ºC (16). We examined carboxysome positioning under high CO_2
113 conditions (2% CO_2) to maximize growth. We found that RbcS-mTQ labeled carboxysomes
114 were equally spaced down the long axis of wild-type *S. elongatus* cells **(Figure 1A)**. The Δ*mcdA*,

115 Δ*mcdB*, and Δ*mcdAB* mutants lost this uniform positioning of carboxysomes **(Figure 1B-D)**; as
116 observed previously at 32ºC (16).
117 We compared the nearest-neighbor spacing of carboxysome foci as a function of cell
118 length **(Figure 1E)**. Wild-type cells showed uniform carboxysome spacing (0.55 ± 0.20 μm)
119 regardless of cell length. All three mutants, on the other hand, displayed a gradual increase in the
120 nearest-neighbor spacing of carboxysome foci as cell length increased. Both the median and
121 variability in spacing were greater in the mutants compared to wild-type **(Figure 1F)**. The
122 increased spacing resulted in fewer carboxysome foci per cell **(Figure 1G)**, and within single
123 cells, there were fewer carboxysome foci per unit cell length **(Figure 1H)**. When quantifying the
124 fluorescence intensity **(Figure 1I)** and size of carboxysome foci **(Figure 1J)**, it became apparent
125 that the increased spacing in all three mutant populations was not likely a result of fewer
126 carboxysomes being assembled, but rather, carboxysomes were coalescing into massive
127 aggregates. Indeed, when comparing carboxysome foci number across cell populations, we find
128 that ~ 95 % of wild-type cells (n = 440) had three or more foci, whereas ~ 80 % of all mutant
129 populations had three or fewer foci **(Figure 1K)**. Roughly 20% of cells from all three mutant
130 populations had a single carboxysome aggregate, whereas wild-type cells never had less than two
131 foci. The 40ºC data shows that the McdAB system not only equally spaces carboxysomes down
132 the cell length, it also serves as an anti-aggregator; preventing carboxysomes from coalescing.
133 We then asked if carboxysome mispositioning affected cell physiology at 40ºC. Wild-
134 type *S. elongatus* cells were 3.1 ± 0.5 microns in length **(Figure 2A)** and 1.25 ± 0.05 microns in
135 width **(Figure 2B)**. We found that Δ*mcdA* cells were of a similar length and width compared to
136 that of wild-type **(Figure 2AB)**. The Δ*mcdB* and Δ*mcdAB* cells had a slightly longer median cell
137 length, but a significantly wider distribution **(Figure 2A)**. These mutants were also thinner

138 compared to wild type **(Figure 2B)**. The presence of both longer and shorter cells suggested
139 asymmetric cell division events. We quantified the frequency of symmetric (mid-cell) versus
140 asymmetric (non-mid-cell) division events and found that asymmetric division was exclusive to
141 the Δ*mcdB* and Δ*mcdAB* populations **(Figure 2C)**. The data show that while both McdA and
142 McdB are required for positioning carboxysomes, the loss of McdB elicits an asymmetric
143 division phenotype at 40ºC.

144 The changes in cell morphology suggested that, even with high CO_2 levels, carboxysome
145 mispositioning may alter cell growth. However, we found only modest reductions in growth rate
146 for all three mutants **(Figure 2D-E)**. Even when grown slowly in ambient CO_2 (0.04%), we did
147 not observe significant differences in growth rate compared to wild-type **(Figure 2F-G)**. Overall,
148 at 40ºC, carboxysomes are mispositioned in all three Mcd mutants, with moderate increases in
149 carboxysome spacing due to aggregation, which ultimately results in fewer carboxysome foci per
150 cell. We found an asymmetric cell division phenotype exclusive to cell without McdB. But in all
151 deletion strains, growth rate was not significantly slower than wild type, with or without CO_2, at
152 this temperature.

153

154 **Carboxysome mispositioning correlates with cell division arrest, cell elongation, and**
155 **asymmetric cell division at 30ºC**

156 We continued our study at 30ºC, a growth temperature closer to what we used to first
157 identify the McdAB carboxysome positioning system (16). As we showed previously, and
158 similar to our 40ºC data, wild-type *S. elongatus* cells have equally spaced carboxysomes **(Figure**
159 **3A)**, while in all three mutants, carboxysomes were mispositioned **(Figure 3B-D)**. Wild-type
160 cells displayed the same carboxysome spacing distance (0.50 ± 0.20 mm) regardless of cell

161 length, while all three mutants had increased carboxysome spacing, and variability in spacing, as
162 cell length increased **(Figure 3E-F)**. Intriguingly, we found that mutant cell lengths were
163 significantly longer compared to wild-type. This cell elongation phenotype was more extreme in
164 the Δ*mcdB* and Δ*mcdAB* mutants, resulting in more distantly spaced carboxysome foci **(Figure**
165 **3F)**. The data once again shows that McdB plays a currently unknown role in carboxysome
166 function, separate from its role in positioning with McdA.

167 The increased spacing resulted in fewer carboxysome foci per cell **(Figure 3G)**, and per
168 unit cell length **(Figure 3H)**. Carboxysome foci in all three mutants were significantly larger
169 than that of wild-type, suggesting aggregation **(Figure 3I-J)**. While ~ 90 % of wild-type cells (n
170 = 486) had three or more foci, ~ 70 % of all mutant populations had three or fewer foci **(Figure**
171 **3K)**. Again, ~ 20 % of cells in all three mutant populations contained a single carboxysome
172 aggregate. This is a striking reduction in carboxysome foci when considering the cell elongation
173 phenotype exclusive to the mutant cell lines.

174 As the carboxysome spacing data suggested, all three mutants had significantly longer
175 cell lengths compared to wild-type when grown at 30ºC **(Figure 4A)**. Median cell width was
176 similar across all strains, however Δ*mcdB* and Δ*mcdAB* cell populations displayed significantly
177 wider distributions in width **(Figure 4B)**. Once again, the Δ*mcdB* and Δ*mcdAB* mutant
178 populations displayed a significant number of asymmetrical division events (~ 70 % of dividing
179 cells) compared to wild-type or Δ*mcdA* **(Figure 4C)**. We propose that carboxysome
180 mispositioning and aggregation at 30ºC elicits cell division arrest, cell elongation and, when
181 McdB is absent, asymmetric cell division; phenotypes that were largely masked when cells were
182 grown at 40ºC.

183 The changes in cell morphology suggested that the mutants may display slower growth
184 rates, even when grown at high CO_2. However, that was not the case. Under high CO_2
185 conditions, no significant reduction in growth rate was observed for all three mutants when
186 compared to wild-type **(Figure 4D-E)**. Even when grown in ambient CO_2, reductions in growth
187 rate of the mutants were minor **(Figure 4F-G)**.
188 Overall, we find that at 30ºC, carboxysomes are mispositioned in the Δ*mcdA*, Δ*mcdB*,
189 and Δ*mcdAB* mutants; with drastic increases in carboxysome spacing due to aggregation,
190 resulting in fewer carboxysome foci per cell. We unveiled a cell elongation phenotype for all
191 three mutant populations, and strikingly, we also found an asymmetric cell division phenotype
192 that was exclusive to cells lacking McdB; a phenotype also found at 40ºC but exacerbated at
193 30ºC **(compare Panel C in Figures 2 and 4)**. Despite these carboxysome aggregation and cell-
194 morphology phenotypes, only minor decreases in growth rate were observed. We propose that
195 carboxysome aggregation decreases the carbon-fixing activity of encapsulated RuBisCO, which
196 triggers an organic carbon-limitation response - cell division arrest, elongation, and asymmetric
197 cell division.
198
199 ***S. elongatus* elongates at 20ºC and this mode of growth is slower in Mcd system mutants**
200 A ten degree drop in growth temperature unveiled the physiological consequences of
201 carboxysome mispositioning at 30ºC, which were largely masked at 40ºC. The catalytic rate of
202 carboxysome-encapsulated RuBisCO is often considered the bottle neck of photosynthesis
203 because the enzyme is inefficient (28) and temperature dependent (20). The light reactions of
204 photosynthesis, however, are considered temperature independent (20, 29). We therefore decided
205 to study the effects of carboxysome mispositioning when cells were grown at 20ºC, which is

206 within the environmentally relevant temperature range - *S. elongatus* PCC 7942 was originally
207 isolated from a fresh water source in the San Francisco bay area, with an annual temperature
208 range of 8ºC to 25ºC (30).

209 Unexpectedly, we found that even wild-type *S. elongatus* undergoes extreme cell
210 elongation when grown at 20ºC **(Figure 5A)**. *S. elongatus* has been previously studied at this
211 temperature (31), but to our knowledge, this is the first time cell morphology has been directly
212 observed. Despite the dramatically long cell lengths, carboxysomes were still robustly aligned
213 down the entire longitudinal axis of the cell **(Figure 5A)**. All three mutants were also elongated,
214 but to a lesser extent, and carboxysomes were clearly mispositioned **(Figure 5B-D)**.

215 Wild-type showed the same uniform carboxysome spacing distance (0.50 ± 0.30 μm)
216 even in cells as along as 20 microns **(Figure 5E)**. All three mutants, on the other hand, displayed
217 dramatically increased carboxysome spacing, and variability in spacing, as cell length increased
218 **(Figure 5F)**. Since all cell types dramatically elongated at 20ºC, the loss of carboxysome
219 positioning resulted in a massive reduction in the number of carboxysome foci per cell **(Figure**
220 **5G)**, and per unit cell length **(Figure 5H)**. Carboxysome foci in all three mutants were
221 significantly larger than that of wild-type, suggesting carboxysome aggregation **(Figure 5I-J)**.
222 While ~ 90% of wild-type cells (n=388) had six or more foci, ~ 80% of all mutant populations
223 had less than five **(Figure 5K)**. The data implicates carboxysome positioning by the McdAB
224 system as a requirement for maximizing carbon-fixation in cells that are elongated when grown
225 at cooler but environmentally relevant temperatures.

226 We quantified cell length at 20ºC and found that the median length of wild-type cells was
227 significantly longer than all three mutant populations **(Figure 6A)**. The Δ*mcdA* cells were
228 similar in width to that of wild-type, while Δ*mcdB* and Δ*mcdAB* cell populations were notably

229 thinner **(Figure 6B)**. Consistent with the wide distributions in cell length **(Figure 6A)**, a
230 significant fraction of division events at this growth temperature were asymmetric across all cell
231 populations. But the frequency of asymmetric division events was still highest in the strains
232 lacking McdB **(Figure 6C)**.

233 When growth rates were assayed at high CO_2 **(Figure 6D-E)** or ambient CO_2 **(Figure 6F-**
234 **G)**, we finally found statistically significant reductions in growth rate for all three mutants when
235 compared to wild-type. However, the reductions in growth rate depended on whether McdA or
236 McdB was absent, and whether the cells were grown with high or ambient CO_2. First, the Δ*mcdA*
237 growth rate was 2-times slower than wild-type at high CO_2 **(Figure 6E)**. But when grown in
238 ambient CO_2, the Δ*mcdA* growth rate was similar to wild-type **(Figure 6G)**. It is known that
239 carboxysome quantity significantly increases when *S. elongatus* is grown in ambient CO_2 (32).
240 Therefore, our data suggest that with ambient CO_2, the greater number of carboxysomes
241 compensates for a loss in their positioning. Alternatively, a decrease in growth rate for Δ*mcdB*
242 and Δ*mcdAB* was found with high- or ambient-levels of CO_2 **(Figure 6E and G)**. The data once
243 again shows that McdB plays a key role in carboxysome function outside of its role in
244 positioning with McdA.

245 Overall, we identified a cell elongation phenotype in wild-type *S. elongatus* cells that
246 occurs when grown at colder, but environmentally relevant temperatures. All three Mcd system
247 mutants elongated to a lesser extent and have aggregated carboxysomes, which resulted in
248 drastically fewer carboxysome foci per cell compared to wild-type. Significant decreases in
249 growth rate were observed, even with high CO_2 present. The findings suggest that in Mcd mutant
250 or wild-type cells, colder growth temperatures decrease the enzyme kinetics of RuBisCO to the
251 point where cell division arrest, elongation, and asymmetric cell division is triggered in response

252 to carbon-limitation. At 30ºC, this response was only found in the Mcd mutants likely due to
253 reduced carbon-fixation efficiency resulting from carboxysome aggregation. At 40ºC, the
254 enzyme kinetics of RuBisCO are fast enough to compensate for carboxysome aggregation, which
255 would explain why Mcd mutants largely displayed cell morphologies and growth rates similar to
256 that of wild-type at higher growth temperatures.
257
258 **McdAB mutants have significantly decreased levels of intracellular RuBisCO**
259 RuBisCO is the sole enzyme providing organic carbon to cellular biomass production and
260 the phototrophic growth of *S. elongatus*. Therefore, we set out to determine if carboxysome
261 mispositioning and the changes in cell morphology of McdAB mutants at 30ºC correlated with
262 altered cellular levels of RuBisCO. Immunoblot analysis against the Large subunit of RuBisCO
263 (RbcL) showed that RuBisCO content is roughly half in all three mutants compared to wild-type
264 cells **(Figure 7A-B)**. RbcL content from cell cultures was normalized based on Atpβ quantity
265 from immunoblot analysis as shown previously (33, 34). The data suggest that although the
266 mutants house massive carboxysome aggregates that are much brighter than those uniformly
267 positioned in wild-type cells **(Supplemental Figure S2)**, the loss of a functioning McdAB
268 system results in a reduction in the total cellular content of RuBisCO.
269 We continued our quantification of cellular RuBisCO content using the RbcS-mTQ
270 fluorescence signal. When quantifying the average RbcS-mTQ intensity per cell, only wild-type
271 seemed to increase RuBisCO content in response to decreasing growth temperature **(Figure 7C)**.
272 This finding is consistent with previous studies showing that RuBisCO abundance in
273 phytoplankton populations (35), including cyanobacterial species (44), inversely correlates with
274 growth temperature. We then normalized the RbcS-mTQ signal to cell length to account for the

275 differences in cell morphology with Mcd system mutants and varying growth temperatures. At
276 40ºC, RuBisCO content was similar across all cell populations, albeit more variable in the
277 mutants **(Figure 7D)**. At 30ºC, all three mutants had roughly 2-fold less RuBisCO compared to
278 that of wild type **(Figure 7E)**; a decrease that is consistent with our immunoblot quantification at
279 32ºC **(see Figure 7B)**. The data confirm that the immunoblot analysis using Atpβ standardization
280 provided a valid measure of cellular RuBisCO abundance, and that the RbcS-mTQ intensity
281 measurements *in vivo* are a reasonable proxy for RuBisCO content. Finally, at 20ºC, all cell
282 populations including wild-type had the lowest levels of RuBisCO content when normalized to
283 cell length **(Figure 7F)** compared to that at higher temperatures **(Figure 7D-E)**. Also, cells
284 without McdB had almost 2-fold less RuBisCO compare to wild-type or Δ*mcdA* cells **(Figure**
285 **7F)**. Overall, our findings suggest that carboxysome mispositioning results in decreased levels of
286 cellular RuBisCO, and unveiled a critical but currently unknown role for McdB in carboxysome
287 integrity and carbon-fixing function.
288

289 **DISCUSSION**

290 We recently identified the McdAB system responsible for the equidistant positioning of
291 carboxysomes in the rod-shaped cyanobacterium *S. elongatus* PCC 7942 (16). We also recently
292 found that McdAB systems are widespread among β-cyanobacteria (17). These findings suggest
293 important and widespread, but currently unknown, physiological roles for carboxysome
294 positioning. Here, we show for the first time that a failure to distribute carboxysomes leads to a
295 number of temperature-dependent changes in cell physiology: decrease in cell growth rate, cell
296 division arrest, cell elongation, asymmetric cell division, and a significant reduction in cellular
297 levels of RuBisCO.

298 At the three temperatures tested (20, 30, and 40ºC), all three mutant cell-types housed
299 few and irregularly spaced carboxysome aggregates, compared to wild-type cells with uniformly-
300 spaced and -sized carboxysome foci. The data here provides quantitative support for our previous
301 findings that the McdAB system equally distributes carboxysomes to opposite sides of the cell to
302 ensure their inheritance following cell division (2, 16), akin to ParA-based plasmid partition
303 systems in bacteria (4). But in addition, and particularly important for protein-based cargoes, the
304 McdAB system serves to prevent carboxysome aggregation. This 'anti-aggregation' activity
305 serves as a homeostasis mechanism that regulates carboxysome size, number, composition,
306 positioning, and ultimately, its carbon-fixing function in the cell. It has recently been found that
307 the pyrenoid, the functional analog of the carboxysome in the chloroplasts of the model alga
308 *Chlamydomonas*, is also spatially regulated and this activity affects carbon-fixation (36). It
309 remains to be seen if other BMCs also use spatial regulation mechanisms to avoid aggregation
310 during their self-assembly to optimize enzymatic efficiency.
311
312 **Physiological defects associated with carboxysome mispositioning are temperature-**
313 **dependent.**
314 Despite the drastic mispositioning and aggregation of carboxysomes in the *mcdA*, *mcdB*,
315 and *mcdAB* deletion strains of *S. elongatus*, only minor changes in cell morphology and growth
316 rate were found when compared to wild-type at the most optimal growth temperature used in this
317 study (40ºC) **(Figures 2)**. At 30ºC however, all three mutants displayed filamentous growth, and
318 a significant fraction of cell division events in the mutant populations lacking McdB were
319 asymmetric **(Figure 4)**. Despite these changes to cell morphology, the growth rates were similar
320 to that of wild-type; even in ambient CO_2. At our coldest but environmentally relevant growth

321 temperature of 20ºC, we found that all cell populations, even wild-type, underwent filamentous
322 growth and asymmetric cell division **(Figure 6)**. Wild-type cells at 20ºC were as much as 5 to
323 10-times longer than the median length when grown at 30ºC or 40ºC. Even in these extremely
324 elongated cells, the McdAB system robustly distributed carboxysomes down the entire cell
325 length **(Figure 5A)**. This mode of filamentous growth was slower in all Mcd system mutants,
326 resulting in significantly shorter filaments compared to wild-type **(Figure 6)**. Overall, we find
327 temperature-dependent physiological defects associated with carboxysome mispositioning and
328 aggregation; phenotypes that were masked at high growth rates and temperatures typically used
329 in the lab, and unveiled at lower but environmentally relevant temperatures.
330

331 **Cell division arrest, filamentation, and asymmetric cell division – A stress response to**
332 **carbon-limitation?**

333 Many bacteria can change shape in response to growth conditions (37). *E. coli* and *B.*
334 *subtilis* produce larger cells under nutrient-rich conditions and smaller cells under nutrient-
335 limited conditions (38, 39). *Pseudomonas aeruginosa* elongates to enhance nutrient uptake
336 during carbon and nitrogen starvation (40); *Caulobacter crescentus* cells increase cell area in
337 response to phosphate starvation (41); and abundant human gut species such as *Bacteriodes*
338 *thetaiotaomicron* elongate under sugar-limited conditions (42). Our findings suggest that *S.*
339 *elongatus* filamentation and asymmetric cell division are responses triggered by organic carbon-
340 limitation, resulting from reduced carbon-fixation activity of RuBisCO in this obligate
341 photoautotroph. Cell filamentation (i) prevents the birth of cells devoid of carboxysomes, (ii)
342 gives the cell an opportunity to increase carbon-fixation by producing more RuBisCO as a larger
343 aggregate, or by nucleating the formation of additional carboxysomes *de novo* elsewhere along

344 the elongated cell and (iii) the increased cell-surface area would increase the light-harvesting
345 capability for photochemistry.

346 A carbon-limitation response parsimoniously explains the two triggers identified here: (1)
347 carboxysome aggregation and (2) colder growth temperatures. What is the mechanism behind the
348 carboxysome aggregation trigger? All Mcd system mutants displayed significant reductions in
349 their total cellular RuBisCO content **(Figure 7)**. Therefore, carboxysome aggregation could
350 trigger the carbon-limitation response simply due to lower levels of RuBisCO as a result of
351 losses in carboxysome integrity and leakage, enzyme stability, and/or degradation. Alternatively,
352 wild-type cells have carboxysomes of a homogenous size, and as cells grow, so do the number of
353 carboxysomes and their net surface area. The net surface area of the carboxysome shell, where
354 RuBisCO substrates and products interface with the cytoplasm, significantly decreases due to
355 carboxysome aggregation. As a result, substrate and product permeability would suffer, which
356 could lead to decreased carbon-fixation rates by encapsulated RuBisCO. It is therefore also
357 possible that the carbon-limitation response is triggered by decreased RuBisCO activity due to
358 decreases in the effective surface area of aggregated carboxysomes. These two proposals are not
359 necessarily mutually exclusive from one another. Consistent with these proposals, it was recently
360 found in Synechococcus sp. PCC 7002 that mispositioning of inactivated carboxysomes towards
361 the cell poles is strongly correlated with their rapid degradation (35).

362 We propose this adaptive response to carbon-limitation is also triggered by low
363 temperature growth, even in wild-type *S. elongatus*. At high temperature (i.e. 40ºC), RuBisCO
364 activity is high (43) and sufficient to compensate for carboxysome mispositioning and RuBisCO
365 aggregation in Mcd system mutants. Therefore, the carbon-limitation response is not triggered.
366 At 30ºC, RuBisCO activity is still high enough to prevent a carbon-limitation response in wild-

367 type cells, but not in Mcd mutants with few and aggregated carboxysomes. As a result, cell
368 filamentation is triggered only in the Mcd mutants. At 20ºC, RuBisCO activity has reduced to a
369 level that, even in wild-type cells, triggers the carbon-limitation response. Mcd mutants are
370 starved for carbon to the point where growth is slowed, resulting in shorter filaments compared
371 to wild-type.
372
373 **Spatial regulation of carboxysomes influences RuBisCO activity and abundance**
374 Psychrophilic phytoplankton species deal with low temperatures, well below the thermal
375 optimum of most enzymes, by increasing the abundance of RuBisCO (35). It has recently been
376 found that low temperature growth (18 to 22ºC) results in increased RuBisCO levels in the
377 marine cyanobacterium *Synechococcus* PCC 7002, compared to growth at 26ºC or 30ºC (44).
378 This trend was also observed in natural phytoplankton assemblages across a wide latitudinal
379 range (35). Consistently, we found here that the RbcS-mTQ signal within carboxysome foci, and
380 within the entire cell, inversely correlated with decreasing growth temperatures.
381 Previous studies have also shown positive relationships between growth rate and
382 RuBisCO abundance (35, 44–48). Elevated carbon fixation rates during blooms in polar regions
383 have been shown to be associated with several-fold increases in RuBisCO. Twenty degrees
384 Celsius is well below the thermal optimum for RuBisCO activity (49), and well below the
385 optimal growth temperature of *S. elongatus*. We therefore conclude that increasing RuBisCO
386 abundance and triggering cell elongation both represent acclimation responses that compensate
387 for the decreased catalytic rate of RuBisCO at low-temperature growth. This response is further
388 compounded when carboxysomes are mispositioned and aggregated in our Mcd mutants. It is
389 important to note that filamentation occurred here under high CO_2 – a condition whereby *S.*

390 *elongatus* does not require the carbon-concentrating activity of carboxysomes for growth (50).
391 Therefore, the evidence further supports that it is not CO_2 substrate limitation causing
392 filamentation, but rather RuBisCO activity that is significantly compromised when complexed in
393 carboxysome aggregates or when cells are grown at colder temperatures. These findings shed
394 light on the importance of the McdAB system in maximizing the carbon-fixation activity of
395 RuBisCO by preventing aggregation during carboxysome self-assembly.
396 Overall, we show that carboxysomes are organized by the McdAB system in
397 cyanobacteria and can appropriately respond to variability in RuBisCO abundance and activity
398 along a wide temperature gradient. Our results suggest that carboxysome homeostasis provided
399 by the McdAB system is part of an autotrophic growth strategy in elongated cells - RuBisCO
400 abundance increases and is distributed into homogeneously-sized carboxysomes at low
401 temperature to overcome the lower catalytic rates of this temperature-dependent enzyme (35).
402
403 **McdB plays a role in carboxysome function outside of its positioning with McdA**
404 Regardless of growth temperature, Δ*mcdB* and Δ*mcdAB* mutants elicited stronger cell
405 elongation and asymmetric division phenotypes compared to Δ*mcdA*. Our findings suggest that
406 McdB plays a currently unknown but critical role in carboxysome function, outside of its role in
407 positioning with McdA. Consistently, our recent bioinformatics analysis of McdAB systems
408 across cyanobacteria identified numerous species with orphan McdBs, once again suggesting
409 functional roles independent of McdA (17). We have also shown previously via bacterial two-
410 hybrid analysis that McdA does not physically associate with any carboxysome component,
411 while McdB directly interacts with a number of shell proteins (16). We have also recently found
412 that purified McdB undergoes Liquid-Liquid Phase-Separation (LLPS) *in vitro* (17). This activity

413 is intriguing given recent studies showing that both α- and β-carboxysomes, as well as the algal
414 pyrenoid, have intrinsically-disordered proteins that from liquid-like condensates with RuBisCO
415 (51–53). Collectively, these studies suggest that LLPS is a common feature underlying
416 carboxysome biogenesis. It is intriguing to speculate that the LLPS activity of McdB and other
417 carboxysome components are related and potentially influence each other.
418
419 **Cold growth temperature triggers elongation and asymmetric cell division**
420 Across the bacterial world, complex systems maintain cell-size homeostasis. We find
421 here that *S. elongatus* maintains cell-size homeostasis when grown at 30ºC or 40ºC, but
422 undergoes filamentation when grown at the environmentally-relevant temperature of 20ºC. A
423 growing number of bacterial species are known to elongate into a filamentous morphology
424 amidst environmental changes to promote survival. For example, *E. coli* cells become
425 filamentous during infection (54, 55), and during DNA damage, the SOS response blocks cell
426 division until damage has been repaired, resulting in elongation (56). Several other forms of
427 stress have been shown to induce elongation, including host environment, antibiotics, nutrient
428 access, pH, heat shock, and osmotic fluctuations (57–60). Bacteria can clearly exist in diverse
429 morphological states, in part dictated by their environment (37, 61).
430 To our knowledge, we find here the first example of bacterial filamentation caused by
431 cold-growth temperature. We propose colder temperatures trigger filamentation indirectly as a
432 carbon-limitation response due to the reduced carbon-fixing activity of RuBisCO. Alternatively,
433 transition into a filamentous morphology has been proposed to confer advantages, such as
434 avoiding phagocytosis via the host immune response (54, 55, 57, 61) or to protect against
435 predation in aquatic environments (58, 62–64). It is attractive to speculate that the growth

436 temperature of 20ºC coincides with the seasonal temperature during which predation occurs (63).
437 That is, *S. elongatus* may use temperature as a cue to elongate so as to avoid planktivorous
438 protists. Consistent with this possibility, previous studies have demonstrated that several
439 freshwater bacteria, including *Caulobacter crescentus* (58), exhibit high phenotypic plasticity
440 and can transition to a filamentous morphology – a transition that may be specifically triggered
441 in the presence of a size-selective protistan predator (63, 65, 66). It is possible that some aquatic
442 bacteria have evolved to undergo filamentation at temperatures that coincide with grazing
443 season.

444 Several studies have characterized the mechanisms by which bacterial filamentation is
445 induced, particularly under DNA damage or exposure to antibiotics (56). But how bacterial cells
446 enter and exit these filamentous states to ensure survival during changes in environment remains
447 poorly characterized and is a recent question of interest. We find here that *S. elongatus* forms
448 filaments when grown at low temperature or when carboxysomes are mispositioned. When these
449 filaments divide, it is asymmetric – forming a daughter cell of 'normal' length. It has been
450 recently shown that *S. elongatus* can also be induced to filament under dim-light stress, and then
451 divides asymmetrically to form daughter cells of the correct size when brought back into well-lit
452 conditions (67). Somewhat related, chlorophyll fluorescence along the cell length of our Mcd
453 mutants was much more heterogeneous, particularly at 20ºC, compared to wild-type **(see Figure**
454 **5A-D)**. It should be noted that in addition to sensing light and inorganic carbon substrates, *S.*
455 *elongatus* responds to lowering temperatures by slowing and even turning off circadian rhythms;
456 thereby down regulating cell growth, division, and metabolic flux (68, 69).

457 The Min system has been shown to play a role in the asymmetric cell division and
458 daughter-cell sizing of filamentous *E. coli* (60), *V. parahaemolyticus* (70, 71), and *S. elongatus*

459 (67). Recent findings suggest that division restoration at the poles of these filaments is regulated
460 by a combination of Min oscillations, FtsZ levels and *terminus* segregation, resulting in daughter
461 cells of the right length (72, 73). The mechanism by which filamentation and asymmetric
462 division occurs in *S. elongatus* is an area of future research. Taken together, the conserved ability
463 for various bacterial species to undergo filamentation and morphological recovery, some of
464 which showing direct selective benefits, strongly suggests that this differentiation plays an
465 important role in survival and proliferation.
466
467
468 **MATERIALS AND METHODS**
469 **Construct designs.** All constructs in this study were generated using Gibson Assembly (74)
470 from synthetized dsDNA and verified by sequencing. Constructs contained flanking DNA that
471 ranged from 500 to 1500 bp in length upstream and downstream of the targeted insertion site to
472 promote homologous recombination into target genomic loci (75).
473
474 **Generation of Bacterial Strains.** All *Synechococcus elongatus* PCC7942 transformations were
475 performed as previously described (75). Plasmid constructs of *mcdA*, *mcdB*, and *mcdAB*
476 deletions were created by replacing the respective coding sequences with a kanamycin resistance
477 cassette. All fluorescent strains were transformed using plasmid pAH40, which contains a
478 chloramphenicol resistance cassette and a second copy of the *rbcS* promoter and gene, attached
479 at the 3' end with the gene encoding for fluorescent protein mTurquoise2 (mTQ) and separated
480 with a GSGSGS linker, inserted into neutral site 1. Transformed cells were plated on BG-11
481 agar. Single colonies were picked into 96-well plates containing 300 µL of BG-11 with 6.35 ug

482 ml^{-1} kanamycin or 3.125 ug ml^{-1} chloramphenicol. Concentrations of both respective antibiotics
483 were gradually increased to 12.5 µg ml^{-1}. Cultures were verified for complete insertion via PCR
484 and removed from antibiotics for experiments.
485
486 **Growth Conditions.** Both wild-type and mutant *Synechococcus elongatus* PCC7942 strains
487 were grown in 125 mL culture flasks (Corning) in 50 mL BG-11 (Sigma) medium buffered with
488 1 g L^{-1} HEPES to pH 8.3 shaken at 130 rpm or on BG-11 plates containing 1.5% (w/v) agar. All
489 strains were maintained and grown under constant LED illumination of 100 µE m^{-2} s^{-1} at either
490 20°C, 30°C, or 40°C in 2% or 0.04% CO_2 as specified. Cultures grown in 0.04% CO_2 were
491 grown in air with no additional CO_2. Cultures were regularly diluted with fresh medium to
492 maintain exponential growth phase for subsequent imaging and immunoblot analyses. For
493 cloning, One Shot™ TOP10 Chemically Competent *E. coli* (ThermoFisher) were grown
494 aerobically at 37° in Luria-Broth medium.
495
496 **Fluorescence microscopy**. Microscopy was performed using exponentially growing cells at an
497 OD of 0.4. Two milliliters of culture were spun down at 15,000 x g for 60 s, resuspended in 100
498 µL of BG-11. Five microliters were transferred to a square 1.5% agarose + BG-11 pad, which
499 was then flipped onto a 35 mm cell culture dish with a #1.5 glass coverslip bottom (ManTek).
500 All images were captured using a Nikon Eclipse Ti2 inverted microscope with a PlanApo
501 Objective lens (100x, 1.45NA, oil immersion), with phase contrast transillumination, and with a
502 SOLA LED light source for imaging chlorophyll fluorescence (Excitation: 560/40nm (540-
503 580nm), Emission: 630/70nm (593-668nm), Dichroic Mirror: 585nm) and RbcS-mTQ
504 fluorescence (Excitation: 436/20nm (426-446nm), Emission: 480/40nm (460-500nm), Dichroic

505 Mirror: 455nm). Images were acquired using a Photometrics Prime 95B Back-illuminated
506 sCMOS Camera. Image analysis was performed using Fiji (76) and the MicrobeJ plugin (77).
507
508 **Growth Curve Measurements.** Cultures were inoculated at a starting OD_{750} of 0.1-0.2 with
509 fresh BG-11. Cell growth was monitored at OD_{750} using a DS-11 Spectrophotometer (DENOVI)
510 at the specified time points. Growth rates were calculated using the linear portion of the
511 exponential phase of growth. Error bars represent the standard deviation from three biological
512 replicates that were recorded from different culture flasks.
513
514 **MicrobeJ quantification.** Multiple fields of view were taken for each cell strain using three
515 channels: Phase contrast provided cell perimeters, and fluorescence microscopy provided
516 chlorophyll autofluorescence and RbcS-mTQ intensities. These data were analyzed using
517 MicrobeJ (77). In each cell-line, cell length detection was performed using the rod-shaped
518 descriptor and thresholding set to 0.4µm < area < max, 0.71µm < width range < 2 µm, 0 µm <
519 width variation < 0.2 µm, and 0 µm < angularity amplitude < 0.35 µm. Carboxysome detection
520 was performed using the point function with a tolerance of 20 and an intensity minimum of 500.
521 Associations, shape descriptors, profiles, and distances were recorded for each strain. All
522 MicrobeJ quantification was also verified manually. Graphs and statistical analyses were
523 generated with Graph Pad Prism.
524
525 **Immunoblot Analysis**. Cells were lysed with a Qsonica sonication system (20 cycles - 30 s on,
526 10s off at 30% power) in 0.5 mL RuBisCO extraction buffer (50 mM EPPS at pH 8.1, 1% PVPP,
527 1 mM EDTA, 10 mM DTT, 0.1% Triton, and sigma protease inhibitor). Laemmli sample buffer

528 (0.1 mL of 4x) was added to lysate prior to loading 10 µL on a 4%–12% Bis-Tris NuPAGE gel
529 (Invitrogen). Gels were transferred onto a Mini-size polyvinylidene difluoride membrane (Bio-
530 Rad) using a Trans-Blot Turbo system (Bio-Rad). The membrane was immunoprobed using
531 rabbit polyclonal antisera against RbcL and the beta subunit of ATP synthase, AtpB (Agrisera)
532 and then goat anti-rabbit IgG secondary antibody (LI-COR). Membrane signals were visualized
533 and quantified at 600 nm using LI-COR Image Studio. For each sample, there were three
534 replicates from the same cell lysate. We normalized RbcL signal using AtpB; a method
535 previously used in Zhang *et al*., 2012 and specifically with *S. elongatus* PCC7942 in Sun *et al*.,
536 2016 (33, 34).
537

538 **ACKNOWLEDGMENTS**

539 We would like to thank Drs. Lyle Simmons, Vincent Denef, and Daniel Ducat for providing
540 critical feedback in experimental direction and data interpretation. We would also like to thank
541 Pusparanee Anne Hakim for experimental assistance and critical reading of the manuscript.
542

543 **REFERENCES**:

544 1. Rae BD, Long BM, Badger MR, Price GD. 2013. Functions, compositions, and evolution
545 of the two types of carboxysomes: Polyhedral microcompartments that facilitate CO2
546 fixation in cyanobacteria and some proteobacteria. Microbiol Mol Biol Rev.
547 2. Savage DF, Afonso B, Chen AH, Silver PA. 2010. Spatially Ordered Dynamics of the
548 Bacterial Carbon Fixation Machinery. Science (80-) 327:1258–1261.
549 3. Kerfeld CA, Melnicki MR. 2016. Assembly, function and evolution of cyanobacterial
550 carboxysomes. Curr Opin Plant Biol 31:66–75.

551 4. Baxter JC, Funnell BE. 2014. Plasmid Partition Mechanisms. Microbiol Spectr 2.
552 5. Badrinarayanan A, Le TBK, Laub MT. 2015. Bacterial Chromosome Organization and
553 Segregation. Annu Rev Cell Dev Biol 31:171–199.
554 6. Viollier PH, Sternheim N, Shapiro L. 2002. Identification of a localization factor for the
555 polar positioning of bacterial structural and regulatory proteins. Proc Natl Acad Sci USA
556 99:13831–13836.
557 7. Perez-Cheeks BA, Planet PJ, Sarkar IN, Clock SA, Xu Q, Figurski DH. 2012. The product
558 of tadZ, a new member of the parA/minD superfamily, localizes to a pole in
559 Aggregatibacter actinomycetemcomitans. Mol Microbiol 83:694–711.
560 8. Thompson SR, Wadhams GH, Armitage JP. 2006. The positioning of cytoplasmic protein
561 clusters in bacteria. Proc Natl Acad Sci USA 103:8209–8214.
562 9. Ringgaard S, Schirner K, Davis BM, Waldor MK. 2011. A family of ParA-like ATPases
563 promotes cell pole maturation by facilitating polar localization of chemotaxis proteins.
564 Genes Dev 25:1544–1555.
565 10. Alvarado A, Kjær A, Yang W, Mann P, Briegel A, Waldor MK, Ringgaard S. 2017.
566 Coupling chemosensory array formation and localization. Elife 6.
567 11. Atmakuri K, Cascales E, Burton OT, Banta LM, Christie PJ. 2007. Agrobacterium
568 ParA/MinD-like VirC1 spatially coordinates early conjugative DNA transfer reactions.
569 EMBO J 26:2540–2551.
570 12. Raskin DM, De Boer PAJ. 1999. Rapid pole-to-pole oscillation of a protein required for
571 directing division to the middle of Escherichia coli. Proc Natl Acad Sci U S A.
572 13. Jordan A, Chandler J, MacCready JS, Huang J, Osteryoung KW, Ducat DC. 2017.
573 Engineering Cyanobacterial Cell Morphology for Enhanced Recovery and Processing of

574 Biomass. Appl Env Microbiol 83.
575 14. Youderian P, Burke N, White DJ, Hartzell PL. 2003. Identification of genes required for
576 adventurous gliding motility in Myxococcus xanthus with the transposable element
577 mariner. Mol Microbiol 49:555.
578 15. Kusumoto A, Shinohara A, Terashima H, Kojima S, Yakushi T, Homma M. 2008.
579 Collaboration of FlhF and FlhG to regulate polarflagella number and localization in Vibrio
580 alginolyticus. Microbiology.
581 16. MacCready JS, Hakim P, Young EJ, Hu L, Liu J, Osteryoung KW, Vecchiarelli AG,
582 Ducat DC. 2018. Protein gradients on the nucleoid position the carbon-fixing organelles of
583 cyanobacteria. Elife 7.
584 17. MacCready JS, Basalla JL, Vecchiarelli AG. 2020. Origin and Evolution of Carboxysome
585 Positioning Systems in Cyanobacteria. Mol Biol Evol 37:1434–1451.
586 18. Shih PM, Wu D, Latifi A, Axen SD, Fewer DP, Talla E, Calteau A, Cai F, Tandeau De
587 Marsac N, Rippka R, Herdman M, Sivonen K, Coursin T, Laurent T, Goodwin L, Nolan
588 M, Davenport KW, Han CS, Rubin EM, Eisen JA, Woyke T, Gugger M, Kerfeld CA.
589 2013. Improving the coverage of the cyanobacterial phylum using diversity-driven
590 genome sequencing. Proc Natl Acad Sci U S A.
591 19. Doney SC, Ruckelshaus M, Emmett Duffy J, Barry JP, Chan F, English CA, Galindo HM,
592 Grebmeier JM, Hollowed AB, Knowlton N, Polovina J, Rabalais NN, Sydeman WJ,
593 Talley LD. 2012. Climate Change Impacts on Marine Ecosystems. Ann Rev Mar Sci.
594 20. Geider RJ. 1987. Light and Temperature Dependence of the Carbon to Chlorophyll a
595 Ratio in Microalgae and Cyanobacteria: Implications for physiology and growth of
596 phytoplankton. New Phytol.

597 21. Raven JA, Geider RJ. 1988. Temperature and algal growth. New Phytol.
598 22. Eppley R. 1972. Temperature and phytoplankton growth in the sea. Fish Bull.
599 23. Chen B, Liu H, Huang B, Wang J. 2014. Temperature effects on the growth rate of marine
600 picoplankton. Mar Ecol Prog Ser.
601 24. Tabita FR, Hanson TE, Satagopan S, Witte BH, Kreel NE. 2008. Phylogenetic and
602 evolutionary relationships of RubisCO and the RubisCO-like proteins and the functional
603 lessons provided by diverse molecular formsPhilosophical Transactions of the Royal
604 Society B: Biological Sciences.
605 25. Sun Y, M Wollman AJ, Huang F, Leake MC, Liu L-N. 2019. Single-Organelle
606 Quantification Reveals Stoichiometric and Structural Variability of Carboxysomes
607 Dependent on the Environment. Plant Cell Adv Publ.
608 26. Ohbayashi R, Nakamachi A, Hatakeyama TS, Watanabe S, Kanesaki Y, Chibazakura T,
609 Yoshikawa H, Miyagishima S. 2019. Coordination of Polyploid Chromosome Replication
610 with Cell Size and Growth in a Cyanobacterium. MBio 10.
611 27. Yu J, Liberton M, Cliften PF, Head RD, Jacobs JM, Smith RD, Koppenaal DW, Brand JJ,
612 Pakrasi HB. 2015. Synechococcus elongatus UTEX 2973, a fast growing cyanobacterial
613 chassis for biosynthesis using light and CO_2. Sci Rep.
614 28. Erb TJ, Zarzycki J. 2018. A short history of RubisCO: the rise and fall (?) of Nature's
615 predominant CO2 fixing enzyme. Curr Opin Biotechnol.
616 29. Ensminger I, Busch F, Huner NPA. 2006. Photostasis and cold acclimation: Sensing low
617 temperature through photosynthesis. Physiol Plant.
618 30. Welkie DG, Rubin BE, Diamond S, Hood RD, Savage DF, Golden SS. 2019. A Hard
619 Day's Night: Cyanobacteria in Diel Cycles. Trends Microbiol.

620 31. Burns RA, MacDonald CD, McGinn PJ, Campbell DA. 2005. Inorganic carbon repletion
621 disrupts photosynthetic acclimation to low temperature in the cyanobacterium
622 Synechococcus elongatus. J Phycol.
623 32. Sun Y, Wollman AJM, Huang F, Leake MC, Liu LN. 2019. Single-organelle
624 quantification reveals stoichiometric and structural variability of carboxysomes dependent
625 on the environment. Plant Cell.
626 33. Sun Y, Casella S, Fang Y, Huang F, Faulkner M, Barrett S, Liu LN. 2016. Light
627 modulates the biosynthesis and organization of cyanobacterial carbon fixation machinery
628 through photosynthetic electron flow. Plant Physiol 171:530–541.
629 34. Zhang P, Eisenhut M, Brandt AM, Carmel D, Silén HM, Vass I, Allahverdiyeva Y,
630 Salminen TA, Aro EM. 2012. Operon flv4-flv2 provides cyanobacterial photosystem ii
631 with flexibility of electron transfer. Plant Cell.
632 35. Young JN, Goldman JAL, Kranz SA, Tortell PD, Morel FMM. 2015. Slow carboxylation
633 of Rubisco constrains the rate of carbon fixation during Antarctic phytoplankton blooms.
634 New Phytol.
635 36. Itakura AK, Chan KX, Atkinson N, Pallesen L, Wang L, Reeves G, Patena W, Caspari O,
636 Roth R, Goodenough U, McCormick AJ, Griffiths H, Jonikas MC. 2019. A Rubisco-
637 binding protein is required for normal pyrenoid number and starch sheath morphology in
638 Chlamydomonas reinhardtii Proc Natl Acad Sci 116:18445 LP –
639 18454.
640 37. Kysela DT, Randich AM, Caccamo PD, Brun Y V. 2016. Diversity Takes Shape:
641 Understanding the Mechanistic and Adaptive Basis of Bacterial Morphology. PLOS Biol
642 14:e1002565.

643 38. Jun S, Si F, Pugatch R, Scott M. 2018. Fundamental principles in bacterial physiology—
644 history, recent progress, and the future with focus on cell size control: a review. Reports
645 Prog Phys 81:056601.
646 39. Sargent MG. 1975. Control of cell length in Bacillus subtilis. J Bacteriol 123.
647 40. Steinberger RE, Allen AR, Hansma HG, Holden PA. 2002. Elongation correlates with
648 nutrient deprivation in Pseudomonas aeruginosa - Unsaturated biofilms. Microb Ecol
649 43:416–423.
650 41. Gonin M, Quardokus EM, O'Donnol D, Maddock J, Brun Y V. 2000. Regulation of stalk
651 elongation by phosphate in Caulobacter crescentus. J Bacteriol 182:337–347.
652 42. Rangarajan AA, Koropatkin NM, Biteen JS. 2020. Nutrient-dependent morphological
653 variability of Bacteroides thetaiotaomicron. Microbiology 166:624–628.
654 43. Galmés J, Hermida-Carrera C, Laanisto L, Niinemets Ü. 2016. A compendium of
655 temperature responses of Rubisco kinetic traits: variability among and within
656 photosynthetic groups and impacts on photosynthesis modeling. J Exp Bot 67:5067–5091.
657 44. Fernández-González C, Pérez-Lorenzo M, Pratt N, Moore CM, Bibby TS, Marañón E.
658 2020. Effects of Temperature and Nutrient Supply on Resource Allocation, Photosynthetic
659 Strategy, and Metabolic Rates of Synechococcus sp. J Phycol.
660 45. Falkowski PG, Sukenik A, Herzig R. 1989. Nitrogen limitation in Isochrysis Galbana
661 (Haptophyceae). II. Relative abundance of chloroplast proteins. J Phycol.
662 46. Raven JA, Johnston AM. 1991. Mechanisms of inorganic-carbon acquisition in marine
663 phytoplankton and their implications for the use of other resources. Limnol Oceanogr.
664 47. Losh JL, Morel FMM, Hopkinson BM. 2012. Modest increase in the C:N ratio of N-
665 limited phytoplankton in the California Current in response to high CO2. Mar Ecol Prog

666 Ser.
667 48. Losh JL, Young JN, Morel FMM. 2013. Rubisco is a small fraction of total protein in
668 marine phytoplankton. New Phytol.
669 49. Galmés J, Aranjuelo I, Medrano H, Flexas J. 2013. Variation in Rubisco content and
670 activity under variable climatic factors. Photosynth Res.
671 50. Cameron JC, Wilson SC, Bernstein SL, Kerfeld CA. 2013. Biogenesis of a Bacterial
672 Organelle: The Carboxysome Assembly Pathway. Cell 155:1131–1140.
673 51. Oltrogge LM, Chaijarasphong T, Chen AW, Bolin ER, Marqusee S, Savage DF. 2020.
674 Multivalent interactions between CsoS2 and Rubisco mediate α-carboxysome formation.
675 Nat Struct Mol Biol 27:281–287.
676 52. Wang H, Yan X, Aigner H, Bracher A, Nguyen ND, Hee WY, Long BM, Price GD, Hartl
677 FU, Hayer-Hartl M. 2019. Rubisco condensate formation by CcmM in beta-carboxysome
678 biogenesis. Nature2019/01/25. 566:131–135.
679 53. Freeman Rosenzweig ES, Xu B, Kuhn Cuellar L, Martinez-Sanchez A, Schaffer M,
680 Strauss M, Cartwright HN, Ronceray P, Plitzko JM, Förster F, Wingreen NS, Engel BD,
681 Mackinder LCM, Jonikas MC. 2017. The Eukaryotic CO2-Concentrating Organelle Is
682 Liquid-like and Exhibits Dynamic Reorganization. Cell 171:148-162.e19.
683 54. Horvath DJ, Li B, Casper T, Partida-Sanchez S, Hunstad DA, Hultgren SJ, Justice SS.
684 2011. Morphological plasticity promotes resistance to phagocyte killing of uropathogenic
685 Escherichia coli. Microbes Infect 13:426–437.
686 55. Justice SS, Hung C, Theriot JA, Fletcher DA, Anderson GG, Footer MJ, Hultgren SJ.
687 2004. Differentiation and developmental pathways of uropathogenic Escherichia coli in
688 urinary tract pathogenesis. Proc Natl Acad Sci 101:1333–1338.

689 56. Kreuzer KN. 2013. DNA Damage Responses in Prokaryotes: Regulating Gene
690 Expression, Modulating Growth Patterns, and Manipulating Replication Forks. Cold
691 Spring Harb Perspect Biol 5.
692 57. Justice SS, Hunstad DA, Cegelski L, Hultgren SJ. 2008. Morphological plasticity as a
693 bacterial survival strategy. Nat Rev Microbiol 6:162–168.
694 58. Heinrich K, Leslie DJ, Morlock M, Bertilsson S, Jonas K. 2019. Molecular basis and
695 ecological relevance of Caulobacter cell filamentation in freshwater habitats. MBio 10.
696 59. Bos J, Zhang Q, Vyawahare S, Rogers E, Rosenberg SM, Austin RH. 2015. Emergence of
697 antibiotic resistance from multinucleated bacterial filaments. Proc Natl Acad Sci 112:178
698 LP – 183.
699 60. Wehrens M, Ershov D, Rozendaal R, Walker N, Schultz D, Kishony R, Levin PA, Tans
700 SJ. 2018. Size Laws and Division Ring Dynamics in Filamentous Escherichia coli cells.
701 Curr Biol 28:972-979.e5.
702 61. Yang DC, Blair KM, Salama NR. 2016. Staying in Shape: the Impact of Cell Shape on
703 Bacterial Survival in Diverse Environments. Microbiol Mol Biol Rev 80:187 LP – 203.
704 62. Wortinger MA, Quardokus EM, Brun Y V. 1998. Morphological adaptation and inhibition
705 of cell division during stationary phase in Caulobacter crescentus. Mol Microbiol 29:963–
706 973.
707 63. Pernthaler J, Zöllner E, Warnecke F, Jürgens K. 2004. Bloom of filamentous bacteria in a
708 mesotrophic lake: Identity and potential controlling mechanism. Appl Environ Microbiol
709 70:6272–6281.
710 64. Pernthaler J. 2005. Predation on prokaryotes in the water column and its ecological
711 implications. Nat Rev Microbiol 3:537–546.

712 65. Hahn MW, Moore ERB, Höfle MG. 1999. Bacterial Filament Formation, a Defense
713 Mechanism against Flagellate Grazing, Is Growth Rate Controlled in Bacteria of Different
714 Phyla. Appl Environ Microbiol 65:25 LP – 35.
715 66. Simek K, Vrba J, Pernthaler J, Posch T, Hartman P, Nedoma J, Psenner R. 1997.
716 Morphological and compositional shifts in an experimental bacterial community
717 influenced by protists with contrasting feeding modes. Appl Environ Microbiol 63:587 LP
718 – 595.
719 67. Liao Y, Rust MJ. 2018. The Min Oscillator Defines Sites of Asymmetric Cell Division in
720 Cyanobacteria during Stress Recovery. Cell Syst.
721 68. Broddrick JT, Welkie DG, Jallet D, Golden SS, Peers G, Palsson BO. 2019. Predicting the
722 metabolic capabilities of Synechococcus elongatus PCC 7942 adapted to different light
723 regimes. Metab Eng.
724 69. Murayama Y, Kori H, Oshima C, Kondo T, Iwasaki H, Ito H. 2017. Low temperature
725 nullifies the circadian clock in cyanobacteria through Hopf bifurcation. Proc Natl Acad
726 Sci U S A.
727 70. Muraleedharan S, Freitas C, Mann P, Glatter T, Ringgaard S. 2018. A cell length-
728 dependent transition in MinD-dynamics promotes a switch in division-site placement and
729 preservation of proliferating elongated Vibrio parahaemolyticus swarmer cells. Mol
730 Microbiol 109:365–384.
731 71. MacCready JS, Vecchiarelli AG. 2018. In long bacterial cells, the Min system can act off-
732 center. Mol Microbiol 109:268–272.
733 72. Raghunathan S, Chimthanawala A, Krishna S, Vecchiarelli AG, Badrinarayanan A. 2020.
734 Asymmetric chromosome segregation and cell division in DNA damage-induced bacterial

735 filaments. bioRxiv 2020.03.16.993485.
736 73. Cayron J, Dedieu A, Lesterlin C. 2020. Bacterial filament division dynamics allows rapid
737 post-stress cell proliferation. bioRxiv 2020.03.16.993345.
738 74. Gibson DG, Young L, Chuang RY, Venter JC, Hutchison CA, Smith HO. 2009.
739 Enzymatic assembly of DNA molecules up to several hundred kilobases. Nat Methods.
740 75. Clerico EM, Ditty JL, Golden SS. 2007. Specialized Techniques for Site-Directed
741 Mutagenesis in Cyanobacteria, p. 155–171. *In* . Humana Press.
742 76. Schindelin J, Arganda-Carreras I, Frise E, Kaynig V, Longair M, Pietzsch T, Preibisch S,
743 Rueden C, Saalfeld S, Schmid B, Tinevez J-Y, White DJ, Hartenstein V, Eliceiri K,
744 Tomancak P, Cardona A. 2012. Fiji: an open-source platform for biological-image
745 analysis. Nat Methods 9:676–682.
746 77. Ducret A, Quardokus EM, Brun Y V. 2016. MicrobeJ, a tool for high throughput bacterial
747 cell detection and quantitative analysis. Nat Microbiol 1:1–7.
748
749
750
751
752
753
754
755
756
757

758 **Table 1**: Strains used in this study

Strain	**Description**	**Source**
Synechococcus elongatus PCC7942	Wild Type	-
Synechococcus elongatus PCC7942	Δ*mcdA*	(16)
Synechococcus elongatus PCC7942	Δ*mcdB*	(16)
Synechococcus elongatus PCC7942	Δ*mcdAB*	(16)
Synechococcus elongatus PCC7942	*rbcS-mTQ*	Wild Type transformed with pAH40
Synechococcus elongatus PCC7942	Δ*mcdA* + *rbcS-mTQ*	Δ*mcdA* transformed with pAH40
Synechococcus elongatus PCC7942	Δ*mcdB* + *rbcS-mTQ*	Δ*mcdB* transformed with pAH40
Synechococcus elongatus PCC7942	Δ*mcdAB* + *rbcS-mTQ*	Δ*mcdA*B transformed with pAH40

759

760

761 **FIGURES**

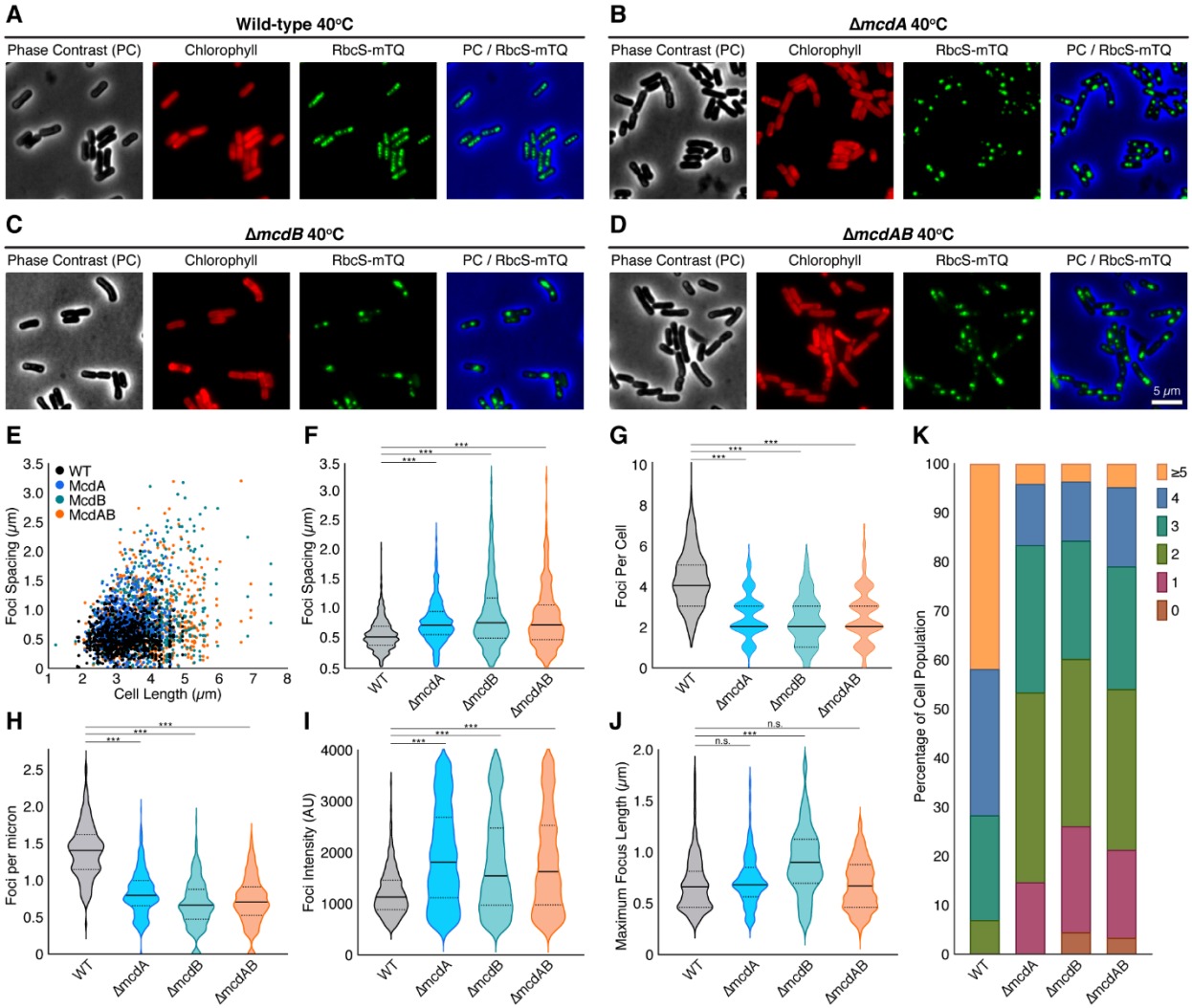

762
763 **Figure 1.** McdAB system mutants display fewer and mispositioned carboxysome aggregates at
764 40°C. (**A-D**) Microscopy images of the specified cell strains grown at 40°C in 2% CO_2. Phase
765 contrast (black), chlorophyll (red), and carboxysomes (green). Phase Contrast (PC) channel is
766 blue in the merge for better contrast. (**E**) Spacing between carboxysome foci as a function of cell
767 length. (**F**) Spacing between carboxysome foci in the same cell. (**G**) Carboxysome foci number
768 per cell. (**H**) Number of carboxysome foci per unit cell length for each strain. (**I**) Carboxysome
769 peak foci intensity for each cell strain. AU = Arbitrary Units. (**J**) Quantification of the maximum
770 length across carboxysome foci. (**F-J**) Solid bars represent the median and dashed lines
771 demarcate the 95% confidence interval. Statistical significance was based on a nonparametric
772 Mann-Whitney test. *** = $P < 0.001$, ** = $P < 0.01$, * = $P < 0.05$, n.s. = not significant. (**K**)
773 Population percentages of cells with the specified number of carboxysome foci. $n \geq 1000$
774 carboxysomes from 440 cells of each strain.
775
776

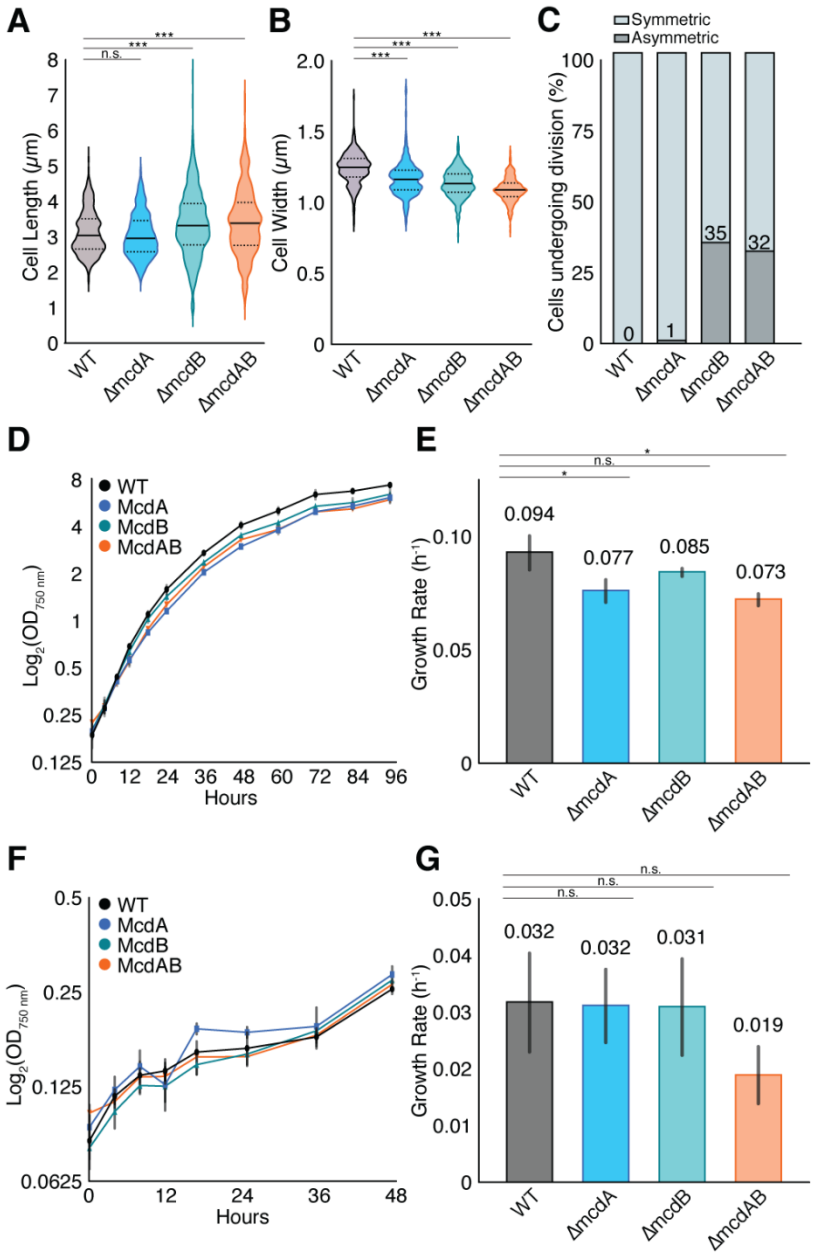

Figure 2. Carboxysome mispositioning correlates with subtle changes in cell physiology at 40°C. (**A**) Cell lengths and (**B**) widths of WT population compared to McdAB system mutants. Cells were grown at in 2% CO_2. n = 440 cells of each strain. Statistical significance was based on a nonparametric Mann-Whitney test. *** = P < 0.001, ** = P < 0.01, * = P < 0.05, n.s. = not significant. (**C**) Percentage of cells undergoing symmetric (mid-cell; light grey bar) or asymmetric (non-mid-cell; dark grey bar) division. (**D**) Growth curves of all strains grown at 40°C in 2% CO_2. (**E**) Quantification of mean exponential growth rate at 40°C in 2% CO_2. (**F**) Growth curves of all strains grown at 40°C in 0.4% CO_2. (**G**) Quantification of mean exponential growth rate at 40°C in 0.4% CO_2. (**D-G**) Error bars represent the standard deviation from three independent biological replicates. Statistical significance was based on an unpaired t-test. *** = P < 0.001, ** = P < 0.01, * = P < 0.05, n.s. = not significant.

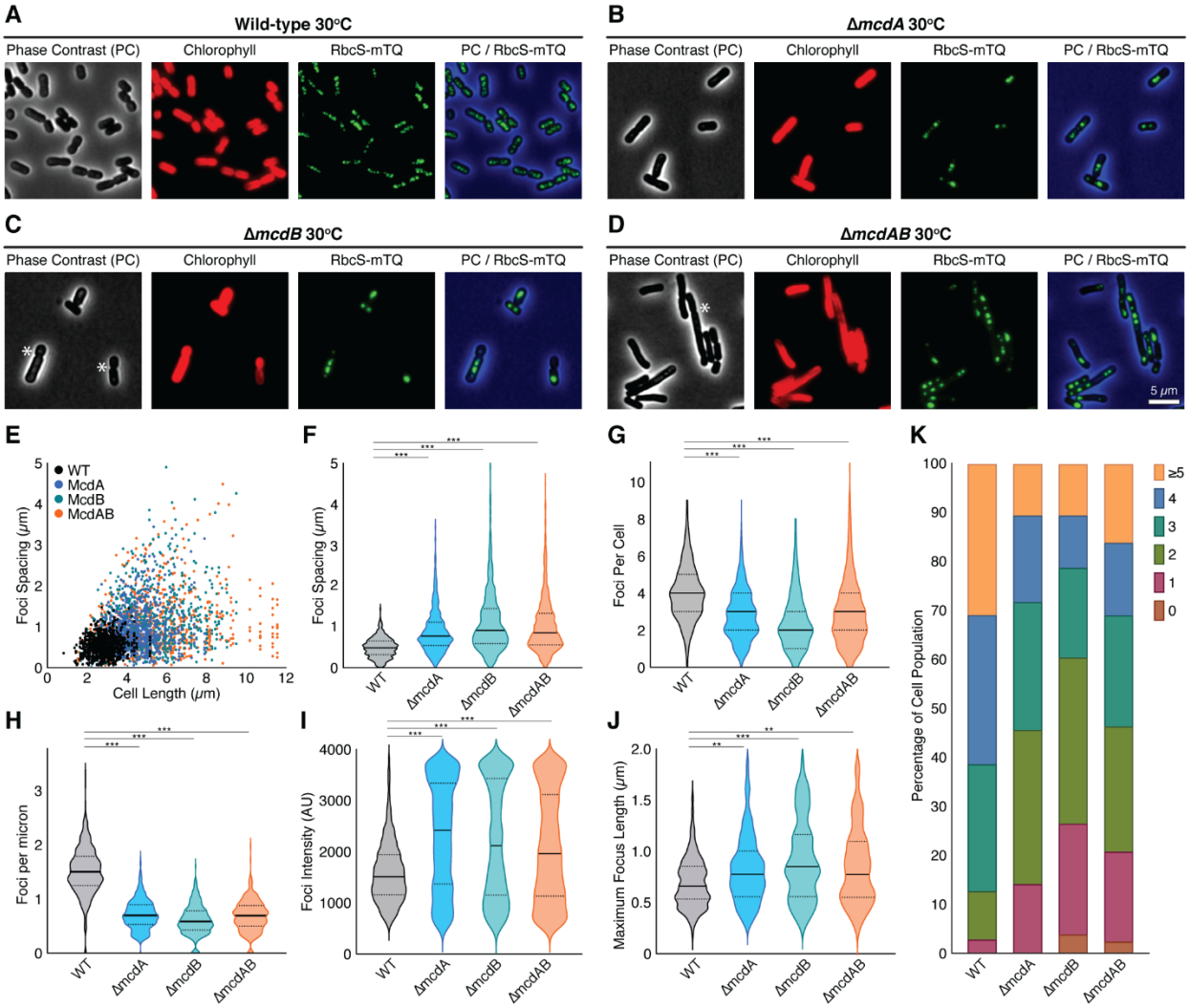

Figure 3. McdAB system mutants house few and mispositioned carboxysome aggregates at 30°C. (**A-D**) Microscopy images of the specified cell strains grown in 2% CO_2. Phase contrast (black), chlorophyll (red), and carboxysomes (green). Phase Contrast (PC) channel is blue in the merge for better contrast. (**E**) Spacing between carboxysome foci as a function of cell length. (**F**) Spacing between carboxysome foci in the same cell. (**G**) Carboxysome foci number per cell. (**H**) Number of carboxysome foci per unit cell length for each strain. (**I**) Carboxysome peak foci intensity for each cell strain. Arbitrary Units (AU). (**J**) Quantification of the maximum length across carboxysome foci. (**F-J**) Solid bars represent the median and dashed lines demarcate the 95% confidence interval. Statistical significance was based on a nonparametric Mann-Whitney test. *** = $P < 0.001$, ** = $P < 0.01$, * = $P < 0.05$, n.s. = not significant. (**K**) Population percentages of cells with the specified number of carboxysome foci. $n \geq 1000$ carboxysomes from 440 cells of each strain.

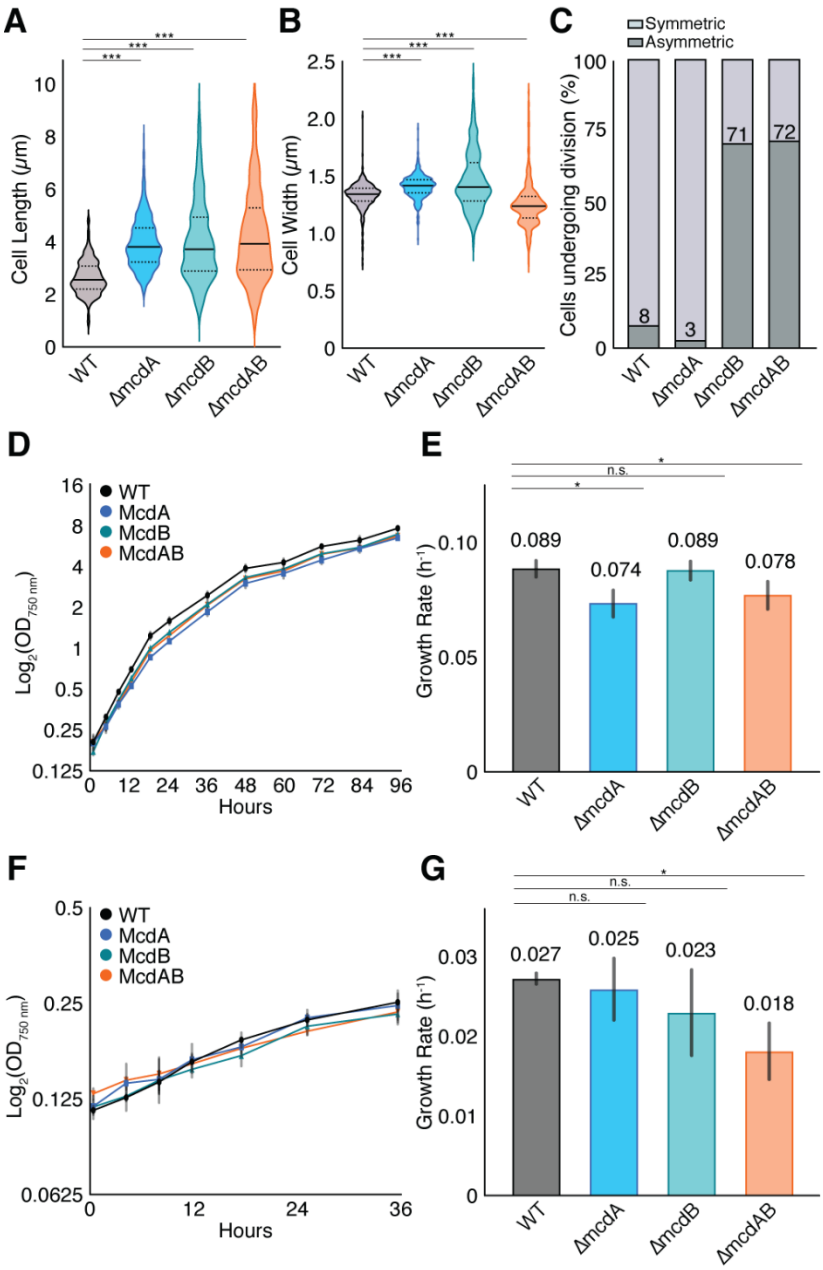

Figure 4. McdAB mutants display cell elongation and asymmetric cell division phenotypes at 30°C. (**A**) Cell lengths and (**B**) widths of WT population compared to McdAB system mutants. Cells were grown in 2% CO_2. n = 440 cells of each strain. Statistical significance was based on a nonparametric Mann-Whitney test. *** = P < 0.001, ** = P < 0.01, * = P < 0.05, n.s. = not significant. (**C**) Percentage of cells undergoing symmetric (mid-cell; light grey bar) or asymmetric (non-mid-cell; dark grey bar) division. (**D**) Growth curves of all strains grown at 30°C in 2% CO_2. (**E**) Quantification of mean exponential growth rate at 30°C in 2% CO_2. (**F**) Growth curves of all strains grown at 30°C in 0.4% CO_2. (**G**) Quantification of mean exponential growth rate at 30°C in 0.4% CO_2. (**D-G**) Error bars represent the standard deviation from three independent biological replicates. Statistical significance was based on an unpaired t-test. *** = P < 0.001, ** = P < 0.01, * = P < 0.05, n.s. = not significant.

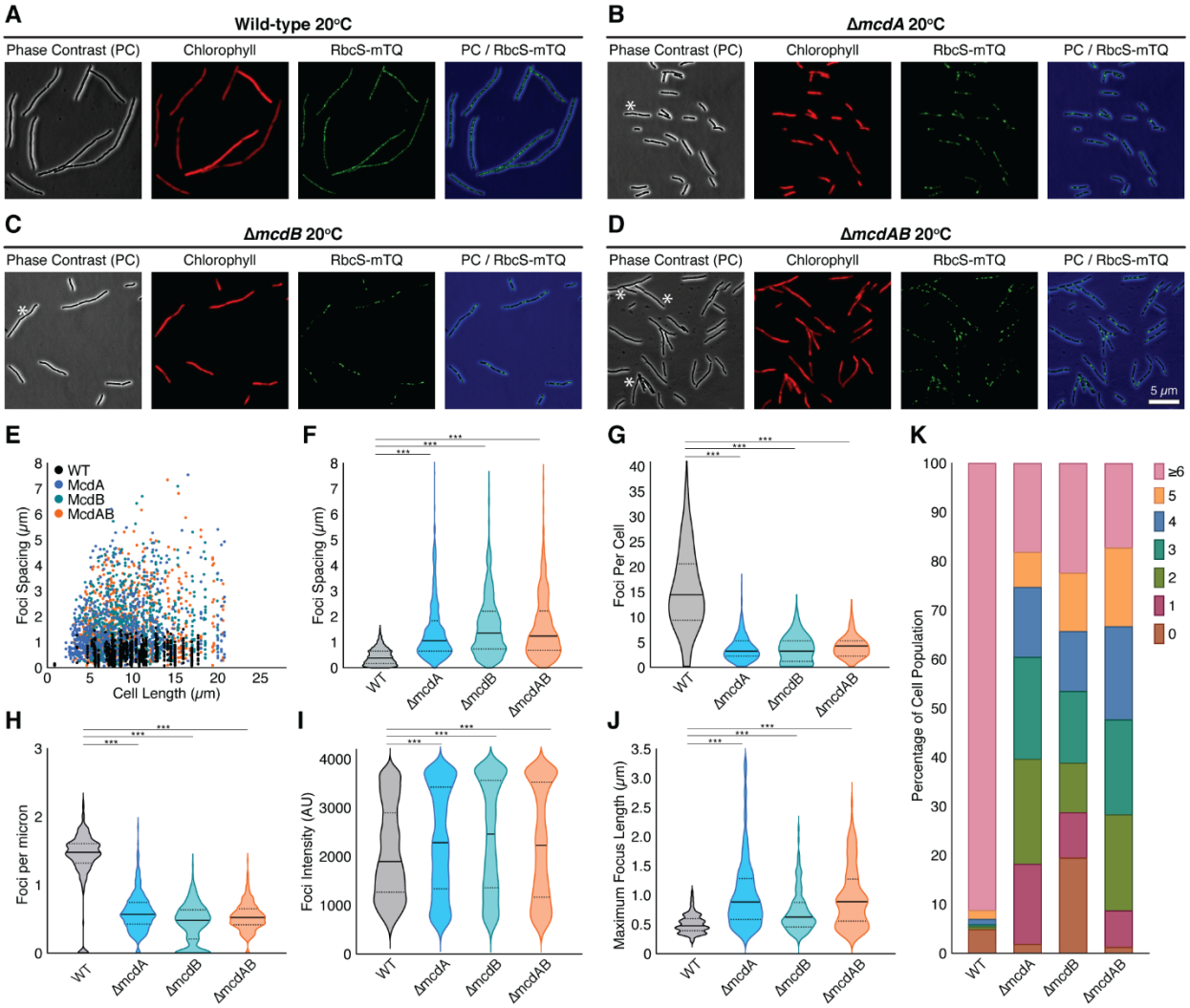

Figure 5. At 20°C wild-type and McdAB system mutants elongate, but only the mutants display few and mispositioned carboxysome aggregates. (**A-D**) Microscopy images of the specified cell strains grown in 2% CO_2. Phase contrast (black), chlorophyll (red), and carboxysomes (green). Phase Contrast (PC) channel is blue in the merge for better contrast. (**E**) Spacing between carboxysome foci as a function of cell length. (**F**) Spacing between carboxysome foci in the same cell. (**G**) Carboxysome foci number per cell. (**H**) Number of carboxysome foci per unit cell length for each strain. (**I**) Carboxysome peak foci intensity for each cell strain. AU = Arbitrary Units. (**J**) Quantification of the maximum length across carboxysome foci. (**F-J**) Solid bars represent the median and dashed lines demarcate the 95% confidence interval. Statistical significance was based on a nonparametric Mann-Whitney test. *** = $P < 0.001$, ** = $P < 0.01$, * = $P < 0.05$, n.s. = not significant. (**K**) Population percentages of cells with the specified number of carboxysome foci. $n \geq 1000$ carboxysomes from 440 cells of each strain.

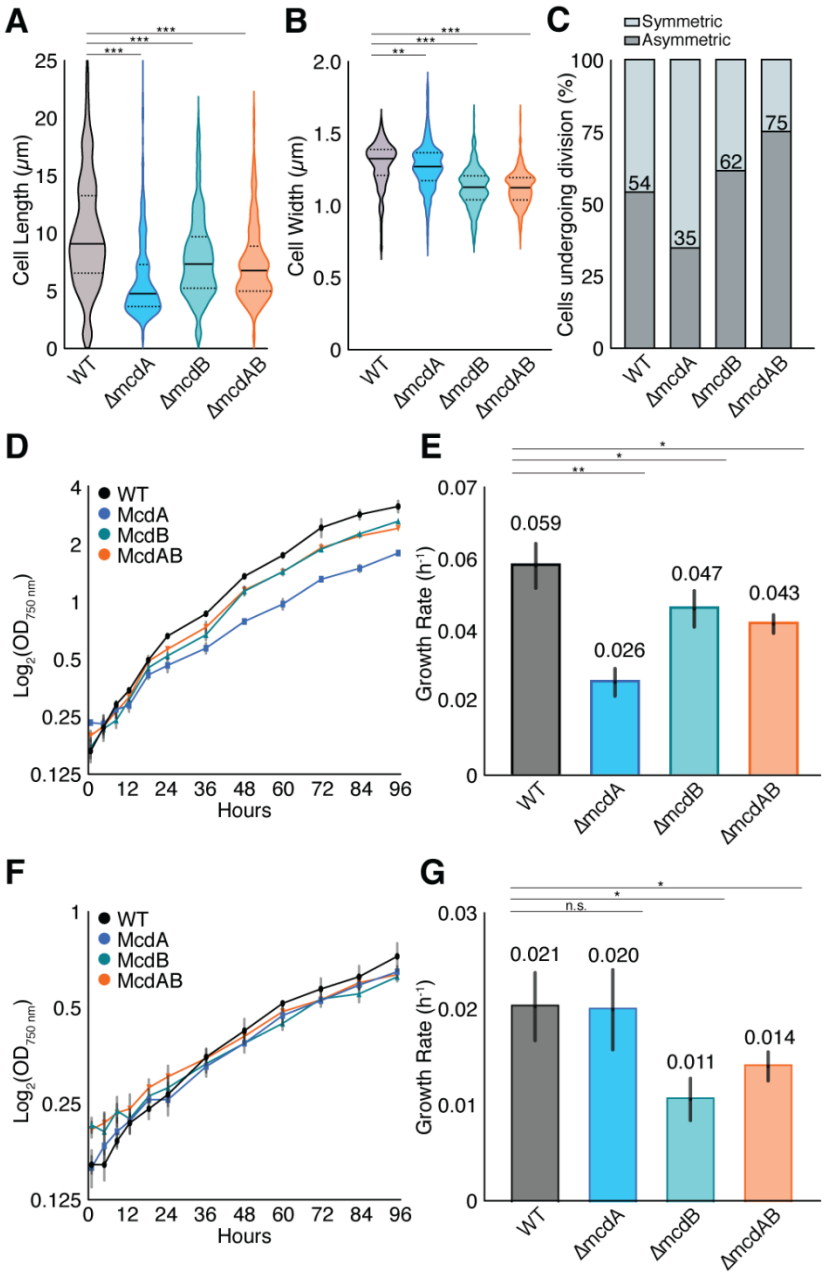

Figure 6. At 20°C wild-type and McdAB mutants elongate and undergo asymmetric cell division, but only mutants show slowed growth rates. (**A**) Cell lengths and (**B**) widths of WT population compared to McdAB system mutants. Cells were grown in 2% CO_2. n = 440 cells of each strain. Statistical significance was based on a nonparametric Mann-Whitney test. *** = P < 0.001, ** = P < 0.01, * = P < 0.05, n.s. = not significant. (**C**) Percentage of cells undergoing symmetric (mid-cell; light grey bar) or asymmetric (non-mid-cell; dark grey bar) division. (**D**) Growth curves of all strains grown at 20°C in 2% CO_2. (**E**) Quantification of mean exponential growth rate at 20°C in 2% CO_2. (**F**) Growth curves of all strains grown at 20°C in 0.4% CO_2. (**G**) Quantification of mean exponential growth rate at 20°C in 0.4% CO_2. (**D-G**) Error bars represent the standard deviation from three independent biological replicates. Statistical significance was based on an unpaired t-test. *** = P < 0.001, ** = P < 0.01, * = P < 0.05, n.s. = not significant.

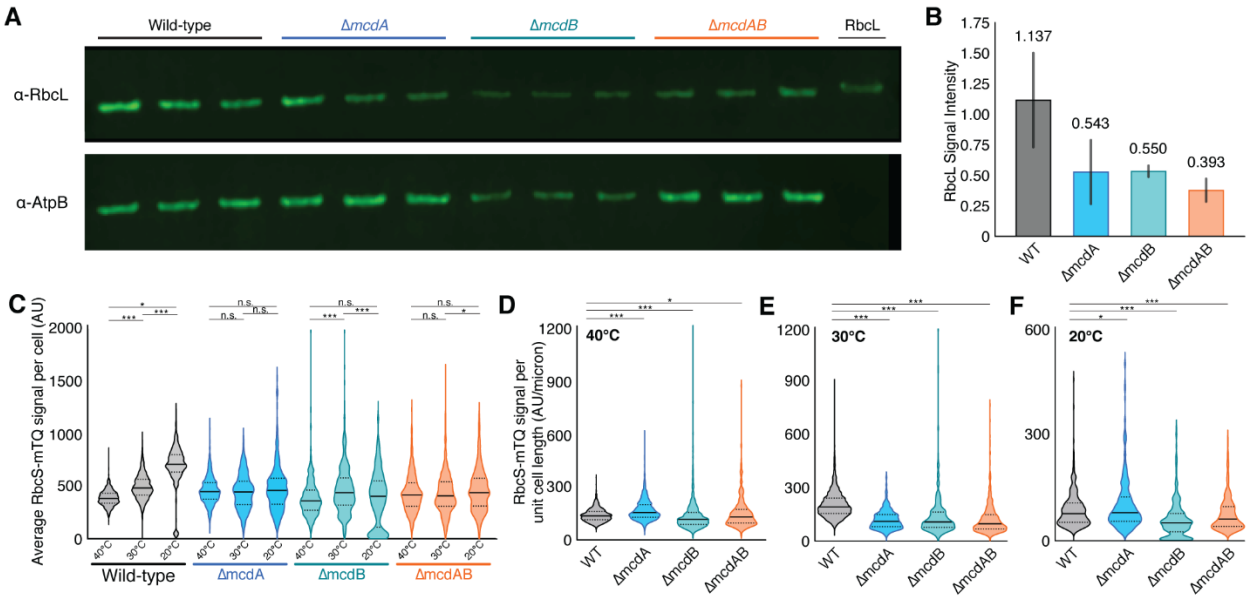

Figure 7. McdAB mutants have decreased cellular levels of RuBisCO. (**A**) Western Blot analysis of RbcL signal (top) and Atpß (bottom). Wild-type (lanes 1-3), Δ*mcdA* (lanes 4-6), Δ*mcdB* (lanes 7-9), and Δ*mcdAB* (lanes 10-12), purified RbcL control (lane 13). (**B**) Quantification of immunoblot signal for the cell type specified normalized against Atpβ signal. Cells were grown at 30ºC in 2% CO_2. Error bars represent the standard deviation from three independent biological replicates. (**C**) Quantification of the average RbcS-mTQ intensity per cell in each strain at the specified temperatures. (**D-F**) Quantification of the average RbcS-mTQ intensity normalized to cell length in each strain at the specified temperatures. n ≥ 338 per cell population. Statistical significance was based on an unpaired t-test. *** = P < 0.001, ** = P < 0.01, * = P < 0.05, n.s. = not significant.

879 **Supplemental Figures**
880

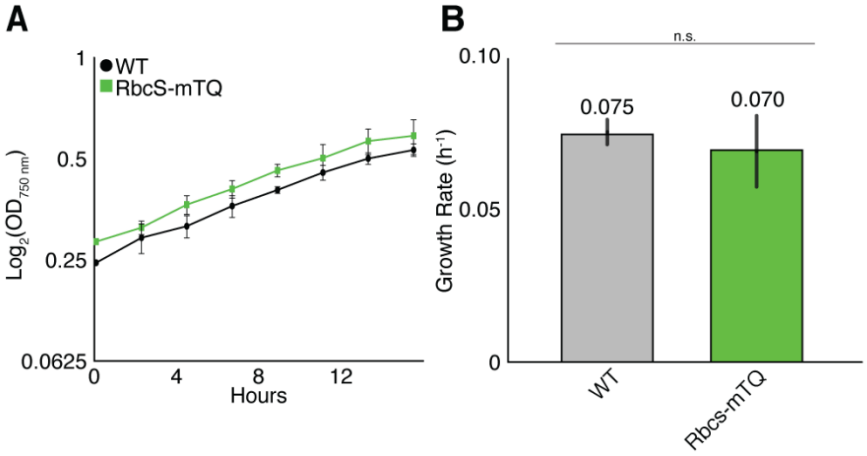

881
882 **Figure S1.** Presence of RbsC-mTQ carboxysome marker does not influence growth. (**A**) Growth
883 curves of wild-type *S. elongatus* with and without RbcS-mTQ carboxysome marker. Cells were
884 grown at 30°C in 2% CO_2. (**B**) Comparison of growth rates. Error bars represent the standard
885 deviation from three independent biological replicates. Unpaired t-test shows growth rates were
886 not statistically different.

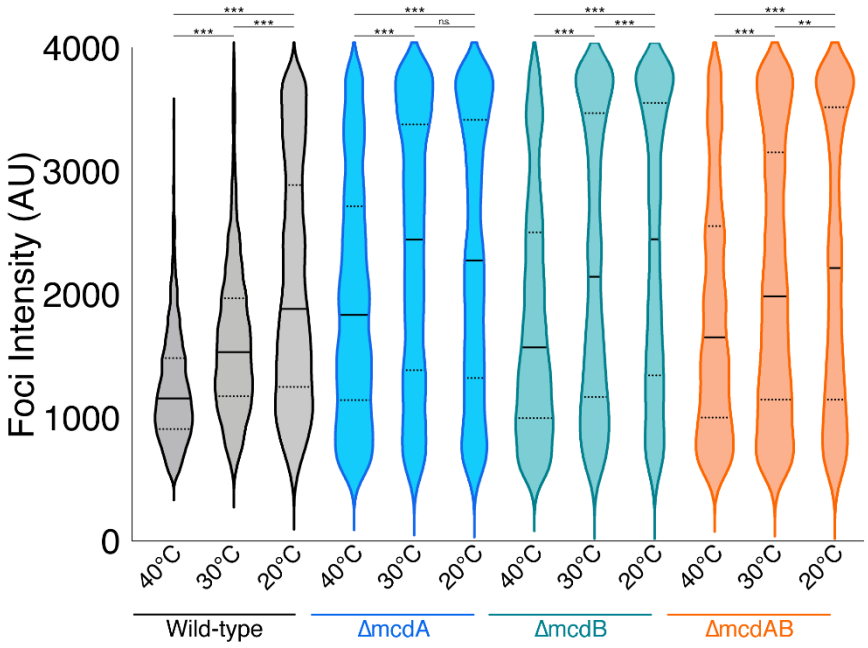

887
888 **Figure S2.** Comparison of the peak RbcS-mTQ foci intensities for each strain across the three
889 growth temperatures tested in this study. AU = Arbitrary Units AU. n > 1000 carboxysomes per
890 cell-line at each temperature. Solid bars represent the median and dashed lines demarcate the
891 95% confidence interval. Statistical significance was based on a nonparametric Mann-Whitney
892 test. *** = P < 0.001, ** = P < 0.01, * = P < 0.05, n.s. = not significant.
893